Chem Circularity

Article

# High-molecular-weight hemp-derived polycannabidiol carbonate thermoplastic with PET-like heat resistance, strength, and processability

## Graphical abstract

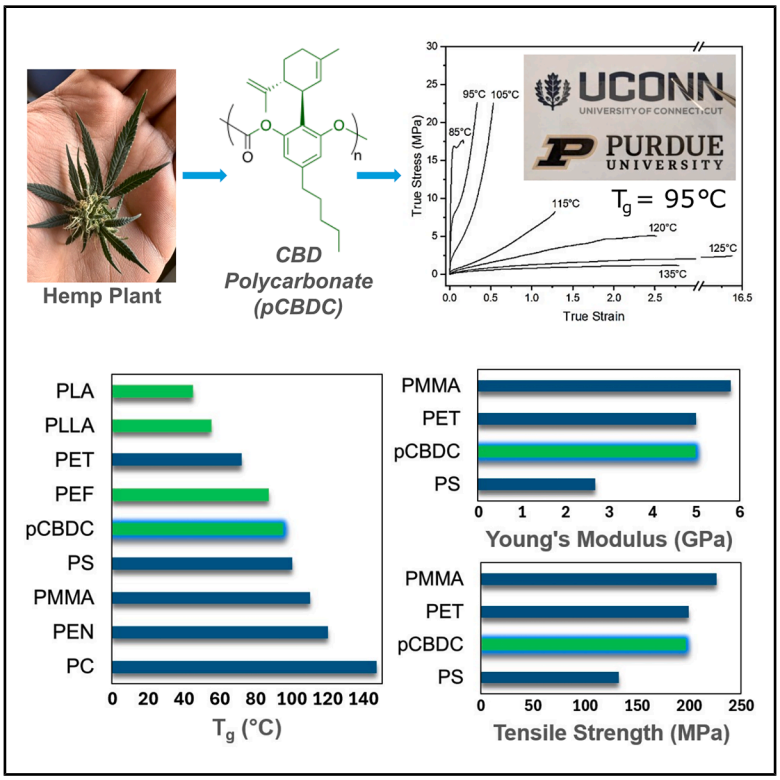


## Highlights

- Hemp-extracted CBD used as is for non-food PET alternative
- Ambient-temperature solution polymerization gives 92% bio-based, 158 kDa Mw polymer
- Oriented films exhibit 5 GPa modulus and 197 MPa tensile strength
- Process-structure-property maps to guide the industrial production of pCBDC films

## Authors

Henry D. Davis, Pritish Aklujkar, Jiahao Mao, ..., Amy Pollock, Gregory A. Sotzing, Mukerrem Cakmak

## Correspondence

g.sotzing@uconn.edu (G.A.S.), cakmak@purdue.edu (M.C.)

## In brief

Replacing PET with renewable alternatives is challenging because few bio-based materials match PET's $T_g$, processability, and low cost. pCBDC is 92% bio-based and has $T_g$, processability, and strength similar to PET. While most bio-based polymers require chemical modification of feedstock before polymerization, CBD extracted from hemp is used directly here, eliminating emissions from modification steps and offering a non-food route to engineering polymers. We also establish processing-structure-property guidelines for industrial production, positioning pCBDC to potentially replace PET in various applications.

Davis et al., 2026, Chem Circularity *1*, 100018
July 7, 2026 
https://doi.org/10.1016/j.checir.2026.100018

CellPress

Please cite this article in press as: Davis et al., High-molecular-weight hemp-derived polycannabidiol carbonate thermoplastic with PET-like heat resistance, strength, and processability, Chem Circularity (2026), https://doi.org/10.1016/j.checir.2026.100018

Chem Circularity

CellPress
OPEN ACCESS

Article

# High-molecular-weight hemp-derived polycannabidiol carbonate thermoplastic with PET-like heat resistance, strength, and processability

Henry D. Davis,[1,5] Pritish Aklujkar,[2,5] Jiahao Mao,[1] Pragati Rout,[3] Ashish R. Khomane,[4] Vishwa Suthar,[2] Amy Pollock,[4] Gregory A. Sotzing,[2,3,*] and Mukerrem Cakmak[1,6,*]

[1]Department of Materials Engineering, Purdue University, West Lafayette, IN, USA
[2]Polymer Program, Institute of Materials Science, University of Connecticut, Storrs, CT, USA
[3]Department of Chemistry, University of Connecticut, Storrs, CT, USA
[4]Materials Science Program, Institute of Materials Science, University of Connecticut, Storrs, CT, USA
[5]These authors contributed equally
[6]Lead contact
*Correspondence: g.sotzing@uconn.edu (G.A.S.), cakmak@purdue.edu (M.C.)
https://doi.org/10.1016/j.checir.2026.100018

**CONTEXT & SCALE** Replacing polyethylene terephthalate (PET) remains a sustainability challenge because few bio-based materials match PET's combination of low cost, high glass transition temperature ($T_g$), and stretch processability needed for industrial film, packaging, and bottle production. Since PET is produced on a massive scale, multiple polymers from different renewable feedstocks will likely be necessary to significantly cut emissions linked to the global PET market. Polyethylene furanoate (PEF) is a promising alternative with similar properties, but its monomers come from food-derived sugars, connecting production to food crop supply chains and land use while requiring several chemical conversion steps that add to carbon emissions. Therefore, finding additional alternatives from non-food feedstocks is important for diversifying renewable supply options. Here, we introduce polycannabidiol carbonate (pCBDC), a 92% bio-based thermoplastic synthesized from cannabidiol (CBD) extracted from hemp biomass, serving as a non-food, renewable, PET-like engineering plastic. pCBDC exhibits high molecular weight, high $T_g$, excellent stretch processability, and high strength. We also establish processing-structure-property relationships that offer guidelines for future industrial manufacturing.

While the properties of pCBDC are promising, its commercial relevance will rely on ongoing declines in CBD feedstock costs. CBD prices have dropped significantly in recent years and are expected to fall further with increased legalization and advances in cultivation, breeding, and extraction. However, because CBD remains considerably more expensive than PET feedstocks, initial pCBDC production would focus on higher-value applications where the polymer cost is a smaller part of the total device cost or where bio-based materials are required or preferred. Further reductions in CBD prices could expand its viable market. This work demonstrates that CBD, a non-food aromatic compound extracted from hemp, can be used directly as a monomer without chemical modification to create a polymer with PET-like $T_g$, mechanical strength, and processability, providing a complementary pathway to PEF to reduce emissions from PET-scale materials.

## SUMMARY

Finding renewable alternatives to polyethylene terephthalate (PET) is challenging, as most bio-based polymers cannot match its combination of glass transition temperature ($T_g$), stretchability, and low cost. Polyethylene furanoate (PEF) shows promise yet relies on food-derived monomers and multistep glucose-to-FDCA conversion, linking supply to food value chains and increasing emissions. Given PET's scale, replacement will likely require non-food polymers to complement PEF. We report polycannabidiol carbonate (pCBDC), a 92% biomass aromatic thermoplastic derived from hemp-based cannabidiol (CBD) without chemical conversion. Synthesized via ambient-temperature solution polymerization, pCBDC achieves high molecular weight (MW; weight-average molecular weight [Mw] = 158 kDa), $T_g$ (95°C), hydrophobicity (contact angle of 102°), and stretchability

Please cite this article in press as: Davis et al., High-molecular-weight hemp-derived polycannabidiol carbonate thermoplastic with PET-like heat resistance, strength, and processability, Chem Circularity (2026), https://doi.org/10.1016/j.checir.2026.100018



**(1,600%). Oriented pCBDC films show modulus (5 GPa) and tensile strength (197 MPa) comparable to oriented PET films. We establish guidelines for industrial pCBDC production by mapping relationships between MW, solution-casting conditions, stretch-processing parameters, and final film properties. These results position pCBDC as a potential alternative to PET, polystyrene (PS), and poly(methyl methacrylate) (PMMA).**

## INTRODUCTION

Identifying renewable, abundant monomers that can be efficiently synthesized and scaled to market demand remains a critical challenge as the plastics industry transitions from petroleum-based materials to sustainable alternatives.[1] This shift is accelerated by increasing environmental, health, and regulatory pressures to reduce carbon emissions and to remove harmful chemicals and additives from consumer products, packaging, and medical devices.[2,3] Bio-based plastics offer promising solutions by reducing fossil fuel dependency and promoting a renewable, circular economy.[4] While researchers have extensively explored melt polymerization of bio-based polymers using metal-based, organic, and enzyme catalysts,[5] for aromatic polymers, these approaches are often impractical for large-scale production, as they are associated with the use of high temperatures (>250°C),[6] catalyst removal difficulties, and purification challenges. Alternative approaches, such as solid-state polymerization,[7] typically achieve only modest molecular weights (MWs; weight-average molecular weight [Mw] ≈ 8–10 kDa),[8] which are insufficient for high-performance applications. Consequently, a critical gap remains in sustainable, aromatic monomers that can deliver high-glass-transition-temperature ($T_g$) aromatic backbones and achieve high MWs (Mw > 50 kDa)[9] through conventional polymerization techniques.

Among engineering polymers, polyethylene terephthalate (PET) is the most challenging to replace. Its unique combination of large-scale production, high $T_g$, and exceptional ability to undergo large draw ratios during uniaxial and biaxial stretching underpins its dominance in both high-end and high-volume applications, from flexible electronics substrates and high-temperature dielectrics to bottles and packaging films.[10,11] In contrast, while some bio-based polymers, such as polyhydroxyalkanoates (PHAs), polylactic acid (PLA), and cellulose acetate (CA), have achieved high MWs, these alternatives often exhibit either low $T_g$ and/or insufficient ductility.[12,13] Bio-PET partially addresses this gap yet remains 70% petroleum based, as terephthalic acid is still petroleum derived.[14] The most promising bio-based PET alternative is polyethylene furanoate (PEF), which offers 100% bio-based content, a slightly higher $T_g$ than PET, and exceptional processing stretchability comparable to PET.[15–17] Because current PEF routes rely on carbohydrate feedstocks, PEF monomer production can, in principle, be rapidly scaled using existing agricultural infrastructure; however, this also keeps PEF production coupled to food and animal feed value chains and potentially sensitive to fluctuations in agricultural commodity markets and land use.[15,16] To complement food-derived PET alternatives such as PEF, there is therefore a strong need for PET-like polymers derived from non-food, bio-based feedstocks that are decoupled from the food supply chain.[15,16] To date, no polymer obtained from a scalable non-food feedstock satisfies PET's unique combination of high $T_g$ and large processing draw ratio, leaving this an unsolved challenge in sustainable polymer science.

To address this need, we introduce polycannabidiol carbonate (pCBDC), a 92% bio-based, amorphous thermoplastic derived from cannabidiol (CBD), an abundant, non-psychoactive aromatic compound extracted from fast-growing hemp biomass (Figures 1A–1C). Hemp can be cultivated across a wide range of temperate and subtropical climates with relatively modest water and little to no pesticide requirements, enabling its cultivation in many areas where food crops grow poorly.[18–22] However, when desired, it can also be integrated into existing crop rotations with corn, soybeans, and small grains, offering agronomic benefits such as improved soil structure and weed suppression.[18,19,23] Industrial hemp is already grown at scale for fiber and seed oil, with agricultural yields around ∼3,400 kg $ha^{-1}$ dry biomass. In this process, CBD is obtained at ∼400 kg $ha^{-1}$ as a co-product from existing extraction streams and then used in pharmaceutical and cosmetic markets.[24] Importantly, CBD from these processes can be directly used in the pCBDC polymerization process without the multistep chemical modifications required by many bio-based polymers (e.g., glucose/sucrose → lactic acid → lactide for PLA and fructose/glucose → HMF → FDCA for PEF), thereby eliminating the greenhouse emissions linked to these intermediary steps.[25,26] Although current global CBD production is not yet enough to fully replace the PET market, industrial hemp acreage is rapidly growing, as hemp is increasingly used for fiber in clothing and construction (insulation and hempcrete) and for food products, such as hemp oil and seeds.[24,27] The legal and geographical restrictions on hemp cultivation are also easing since hemp is now legally grown in many countries—including the United States, Canada, the European Union, China, and parts of Africa and Latin America—under regulations that limit THC content to below 0.3 wt %.[28,29] These rules clearly differentiate industrial hemp from psychoactive cannabis and have helped establish a growing global supply chain. Therefore, pCBDC can complement other bio-based polymers, such as PEF, to diversify supply chains and reduce the impact of market fluctuations or sector-specific changes.

pCBDC is synthesized via scalable, ambient-temperature solution polymerization, using commercial triphosgene (a crystalline solid) as a co-monomer in place of hazardous phosgene gas. Ambient temperature and basic conditions suppress phosgene evolution, while complete triphosgene consumption leaves only carbonate linkages in the polymer backbone. This method yields a high Mw of 158 kDa, excellent processability, and optical clarity. The resulting polymer exhibits a $T_g$ of 95°C arising from its rigid aromatic backbone (20°C higher than PET), remarkable processing stretchability of up to 1,600% (comparable to PET), modulus and tensile strength of 5 GPa and 197 MPa in the oriented state (equivalent to oriented PET), and pronounced

Please cite this article in press as: Davis et al., High-molecular-weight hemp-derived polycannabidiol carbonate thermoplastic with PET-like heat resistance, strength, and processability, Chem Circularity (2026), https://doi.org/10.1016/j.checir.2026.100018





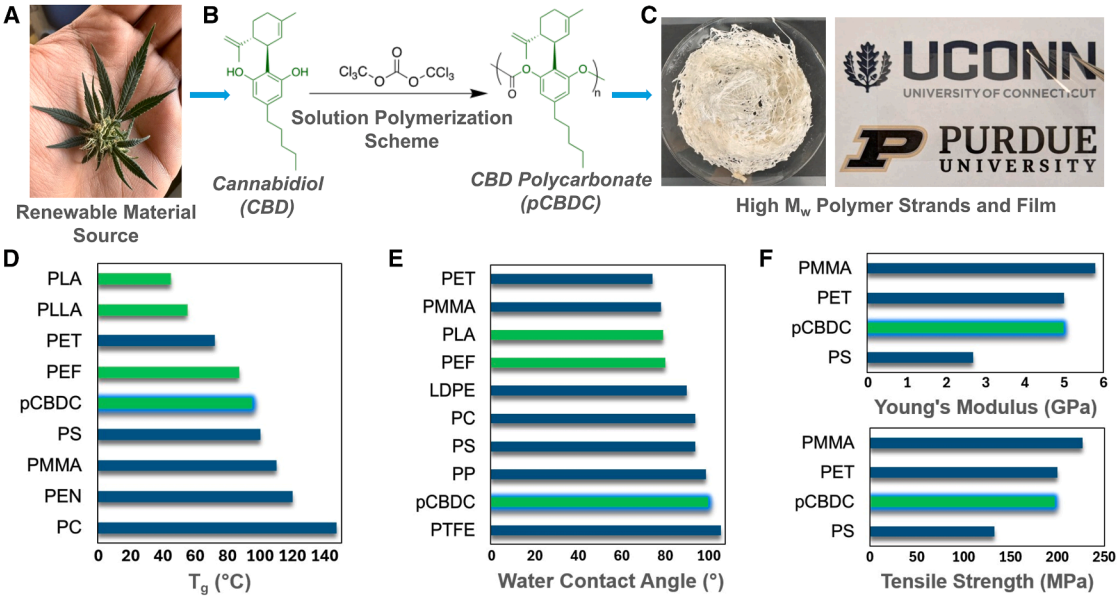


**Figure 1. pCBDC synthesis and properties**

(A) Industrial hemp as a renewable raw material source.

(B) Polymerization scheme for pCBDC.

(C) Isolated high-MW polymer for processing studies.

(D) Glass transition temperature of various polymers vs. pCBDC (petroleum-based shown in blue and bio-based shown in green).

(E) Water contact angle of various polymers vs. pCBDC.

(F) Young's modulus and tensile strength of uniaxially oriented films made from various polymers vs. pCBDC.

hydrophobicity with a water contact angle of 102°. One of the keys to the success of PET is the desirable strain hardening it shows during stretching due to strain-induced crystallization. This strain hardening allows PET to stretch to large draw ratios during processing while maintaining uniform film thickness. Although amorphous, pCBDC also exhibits strain hardening during processing due to its high MW. Additionally, the amorphous nature of pCBDC makes it more desirable than semi-crystalline polymers for some applications, such as injection molding, as it undergoes less shrinkage and cools more quickly, enabling higher dimensional fidelity and shorter cycle times. In contrast, crystal formation causes shrinkage and heat generation.[30,31] Although pCBDC is chemically a polycarbonate rather than a polyester, its $T_g$ and processing draw ratio more closely resemble those of PET than BPA-based polycarbonate. pCBDC's combination of scalability, properties, and processability positions it to replace PET and other engineering polymers—such as polystyrene (PS) and poly(methyl methacrylate) (PMMA)—in many demanding applications, including flexible electronics substrates and high-temperature insulation and dielectrics, as well as in high-volume products, such as bottles, food packaging, and fibers, as feedstock prices decrease.

The economic case for pCBDC and other CBD-based polymers developed in our lab[32] is rapidly strengthening, as the price of CBD has dropped precipitously, driven by expanded hemp cultivation, genetic improvements to increase CBD content, and advances in extraction technologies.[33,34] Since its price exceeds commodity plastic resins (~1–1.5 USD $kg^{-1}$),[35] pCBDC will initially find use in higher-value applications—such as flexible electronic substrates and high-temperature dielectrics—where the polymer cost is a smaller fraction of total device cost and in cases where a more sustainable product is desired. Further scale-up of hemp cultivation, driven by clearer legal status, higher CBD yields, and improved extraction, is expected to continue reducing feedstock costs and broaden the economically accessible application space over time.[34,36] Additionally, in spaces where consumers request bio-based alternatives, pCBDC price only needs to compete with current bio-based options such as PEF, which has a price of ~7.5 USD $kg^{-1}$.[37]

To fully realize the potential of pCBDC, it is essential to understand how MW and processing conditions dictate the final film structure and properties. Polymer chain orientation has a significant impact on film quality, with higher orientation typically leading to increased strength, decreased gas permeability, and improved dielectric properties.[38–40] Previous research on solution casting of amorphous polymers has shown that chain alignment in the final film increases with lower solution concentration, lower casting thickness, lower drying air temperature, higher air speed, and higher MW.[41–46] Studies on uniaxial stretching have shown that higher-MW films exhibit greater chain alignment and stronger strain hardening, leading to more uniform-thickness films.[47–55] Moreover, stretching rate and temperature significantly impact achievable draw ratios and final film properties, including thickness uniformity and polymer chain orientation. For amorphous polymers such as pCBDC, optimal stretching occurs between $T_g$ and the liquid-liquid transition temperature ($T_{ll}$) and is typically around $T_g$ + 20°C–30°C.[46,48,56,57] Stretching too close to $T_g$ can lead to micro-void formation,[58,59] while stretching above $T_{ll}$ results

Please cite this article in press as: Davis et al., High-molecular-weight hemp-derived polycannabidiol carbonate thermoplastic with PET-like heat resistance, strength, and processability, Chem Circularity (2026), https://doi.org/10.1016/j.checir.2026.100018



in viscous behavior with little strain hardening, leading to non-uniform thickness.[54,56] However, between $T_g$ and $T_{II}$, the polymer behaves as a structured fluid, with partial segmental ordering[60–62] that works synergistically with entanglements during stretching to induce superior chain alignment and intense strain hardening,[46,48,56,57] both of which are critical in processes such as tenter-frame biaxial stretching for substrates and films, thermoforming for packaging, and stretch blow molding for bottles.

To establish foundational guidelines for the industrial processing of pCBDC, we systematically investigate how MW and processing parameters govern the polymer's structure and resulting film properties. While industrial production will utilize melt processing to eliminate the long-term use of solvents, this study focuses on real-time analysis during solution casting, given limited material quantity, to examine how MW, solution concentration, casting thickness, and drying temperature affect polymer chain alignment and film quality. We further employ real-time mechano-optical measurements during uniaxial stretching to determine the $T_{II}$ and identify optimal conditions for achieving large draw ratios and for maximizing chain alignment and strain hardening. Finally, we measure the mechanical properties of as-cast and oriented films and compare them to PET, PS, PMMA, and PEF. These processing-structure-property relationships establish critical guidelines for producing high-quality pCBDC films, positioning this polymer as a scalable, renewable alternative for both premium and high-volume applications where conventional materials currently dominate.

## RESULTS AND DISCUSSION

### Polymer synthesis and chemical analysis

The synthesis of pCBDC was performed by solution polymerization at ambient temperature, using triphosgene as a crystalline co-monomer with CBD in the presence of pyridine as a base catalyst and dichloromethane (DCM) as the solvent (Figures 1A–1C). Proton NMR ($^1$H-NMR) (Figure S1) provides structural confirmation of the polymer, with characteristic resonances corresponding to the shift in aromatic protons of CBD due to the presence of carbonate linkages. Stacked spectra of CBD and pCBDC (Figure S2) show the shift and absence of hydroxyl protons between 6 and 6.5 ppm.[32,63] The alicyclic-aromatic architecture inherent to CBD was retained, providing a unique combination of rigidity and conformational mobility within the repeat units. The hybrid aromatic-aliphatic architecture of pCBDC maintains a high $T_g$ while simultaneously enabling large processing draw ratios. Gel permeation chromatography (SEC) analysis revealed that the polymerization can afford high-MW products (Mw up to 158 kDa) with relatively narrow dispersity—essential for chain entanglement and achieving large draw ratios in subsequent processing (Figure S3).

As hydrophobicity can improve moisture resistance, stability, and performance of flexible electronics substrates and dielectric materials, especially in high-humidity environments,[64] surface wettability measurements were performed on pCBDC films using a sessile drop method. As shown in Figure 1E, untreated pCBDC films exhibit a water contact angle of 102°, surpassing those of many commodity petroleum and bio-based polymers and approaching values typical of hydrophobic engineering plastics.[65] This enhanced hydrophobicity is attributed to the densely packed, alicyclic-aromatic architecture, which minimizes polar surface groups accessible to water. Taken together with the high $T_g$ (Figure 1D), these results establish pCBDC as a rare example of a bio-based polymer that unites scalability, high MW, hydrophobicity, high $T_g$, and large draw ratio.

### Sustainability, circularity, and life cycle considerations

Critical to the development of this polymer, we evaluate the sustainability, circularity, and life cycle considerations of pCBDC to investigate its potential as a next-generation engineering thermoplastic. pCBDC incorporates chemically recyclable carbonate linkages that enable depolymerization by multiple nucleophile-mediated pathways, including hydrolysis and alcoholysis, supporting potential monomer recovery consistent with closed-loop recycling frameworks established for condensation polymers.[66–69] As a high-performance, hydrophobic thermoplastic engineered for durable applications, pCBDC is not intended for rapid environmental biodegradation that could compromise material lifetime and functional performance. Instead, its circularity derives from controlled recovery pathways, including chemical recycling and mechanical reprocessing.[70–72] This durability-recyclability balance is increasingly recognized as a more effective sustainability strategy for engineering plastics than uncontrolled degradation. When coupled with a renewable hemp-derived monomer, these attributes position pCBDC within an emerging circular materials framework.

A comprehensive life cycle assessment (LCA) and techno-economic analysis (TEA) will ultimately be required to quantify environmental benefits; however, rigorous evaluation at this developmental stage would depend on uncertain assumptions regarding agricultural productivity, feedstock pricing, solvent recovery efficiencies, and manufacturing scale.[4] Rather than presenting speculative metrics, we identify the parameters most likely to govern life cycle performance. Feedstock costs have declined with expanded hemp cultivation and improved extraction technologies and are expected to decrease further as supply chains mature.[24,27,33] Moreover, the combination of scalable polymerization, high MW, and a chemically recyclable backbone supports long service lifetimes and material recovery. These factors are dominant contributors to favorable life cycle outcomes for engineering plastics.

In the synthesis of pCBDC, triphosgene was employed to enable access to engineering-level MWs required for chain entanglement, stretch processability, and mechanical robustness. As a stable crystalline solid that is fully consumed during polymerization, triphosgene offers safer handling than phosgene gas and provides a practical route to establish the performance envelope of this emerging polymer system. While carbonate transesterification strategies using dimethyl or diphenyl carbonate offer attractive long-term pathways aligned with greener synthesis principles, such equilibrium-limited processes often struggle to achieve comparable MWs without extensive optimization. Accordingly, the current approach should be viewed as a developmental benchmark rather than a fixed polymerization strategy. Ongoing efforts are directed toward more sustainable polymerization strategies, including functionalized CBD monomers, $CO_2$-derived intermediates, and melt polymerization processes, to further

Please cite this article in press as: Davis et al., High-molecular-weight hemp-derived polycannabidiol carbonate thermoplastic with PET-like heat resistance, strength, and processability, Chem Circularity (2026), https://doi.org/10.1016/j.checir.2026.100018



CellPress
OPEN ACCESS

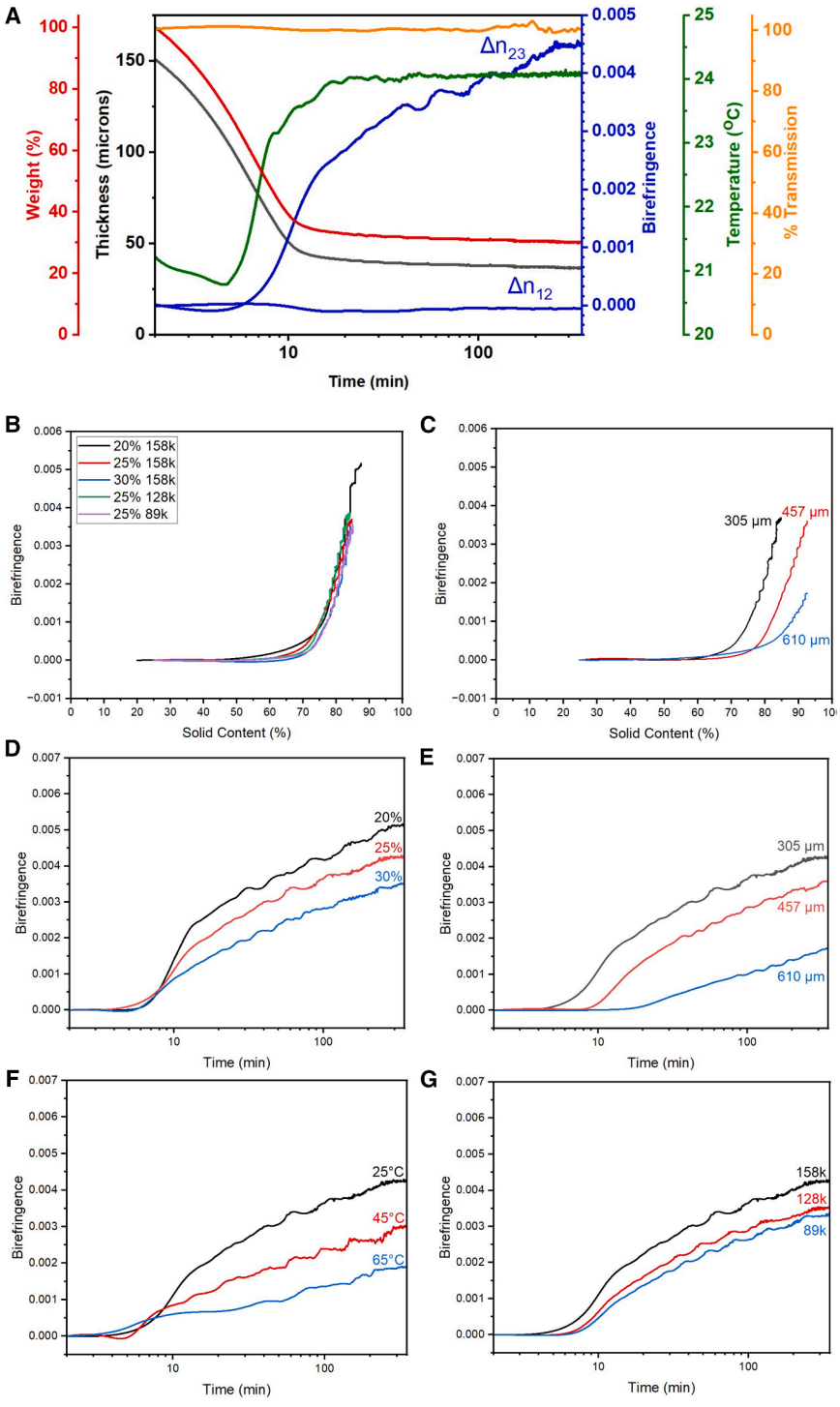


**Figure 2. Real-time drying analysis during solution casting**

(A) Quantities measured while drying a solution-cast pCBDC film with Mw = 158 kDa, 25% solid content, and 305 μm casting thickness; drying in room temperature air at 1 m/s $\Delta n_{12}$ is in-plane birefringence, and $\Delta n_{23}$ is out-of-plane birefringence.

(B and C) Plots of birefringence vs. solid content for (B) various concentrations and MWs and (C) various thicknesses.

(D–G) The effect of varying parameters on out-of-plane birefringence development during drying of pCBDC film with base parameters set at Mw = 158 kDa, 25% solid content, 305 μm casting thickness, and room temperature air at 1 m/s. Varied parameters: (D) solid content, (E) doctor blade gap thickness, (F) air temperature, and (G) polymer MW.

reduce solvent use, hazardous reagents, and overall environmental impact while maintaining high performance.

## Solution casting with real-time drying analysis

Films were cast and dried under varied parameters to determine the effects of MW, solution concentration, casting thickness, and drying temperature on birefringence levels during drying using an instrumented system (shown in Figure S6). A typical combined plot showing real-time quantities measured during a single experiment is shown in Figure 2A. During the initial portion of the drying process, the solvent rapidly evaporates until most of it is gone, after which evaporation slows considerably for the remainder of the drying process. This rapid solvent evaporation pushes the film temperature below the air temperature via evaporative cooling until it equilibrates with the air as the evaporation rate slows. After sufficient solvent has evaporated, the out-of-plane (OOP) birefringence ($\Delta n_{23}$) begins to increase and then levels off. This increase in OOP birefringence is due to the anisotropic shrinkage of the film during drying. Because the film is constrained in the $x$ and $y$ directions by the substrate, solvent evaporation causes it to shrink preferentially in the thickness ($z$) direction.

Additionally, as the solid content reaches a critical concentration of ~70%–75% for most conditions, as shown in Figure 2B, chain relaxation is suppressed, and further solvent evaporation compresses the chains in the $z$ direction, leaving them preferentially oriented parallel to the film plane as seen by a linear increase in OOP birefringence with solid content. After some time, the film stops densifying, and the OOP birefringence begins to level off. Throughout this process, the in-plane birefringence ($\Delta n_{12}$) remains near zero, indicating in-plane isotropy even as OOP anisotropy increases.

The critical solid concentration at which birefringence starts increasing is consistent across different solid concentrations

Please cite this article in press as: Davis et al., High-molecular-weight hemp-derived polycannabidiol carbonate thermoplastic with PET-like heat resistance, strength, and processability, Chem Circularity (2026), https://doi.org/10.1016/j.checir.2026.100018



and MW, as shown in Figure 2B. However, for films of different thicknesses, the critical concentration increases from ~70% for 305 μm to ~85% for 610 μm. This could be due to skin formation in thicker films, which increases the film's average solid concentration, even as the bulk portion of the film below the skin has a lower solid concentration than the skin. Because the rapid birefringence increase would only be seen when the bulk portion of the film reaches the critical concentration, the average solid concentration at birefringence increase will be higher in thicker films than in thinner films.

As polymer chain orientation is critical to high-quality films, the effect of processing parameters on birefringence development is systematically illustrated across Figures 2D–2G and described in the following paragraphs.

Solution concentration (Figure 2D): lower-concentration solutions exhibit a more rapid initial increase in birefringence and higher final birefringence than higher concentrations. A potential cause of the reduced birefringence at higher concentrations is that, although all films have similar initial thicknesses, the lower concentration has a lower final thickness because it contains less solid material; therefore, it experiences greater *z*-direction compression, leading to higher chain alignment.

Casting thickness (Figure 2E): thinner films exhibit an earlier onset of birefringence increase, a steeper initial rise in birefringence, and a higher final birefringence. This can be explained by the fact that although the surface area and corresponding evaporation rate in each condition are the same, thicker films contain a larger total solvent volume. As a result, the solvent concentration decreases more quickly in thinner films, leading to rapid compression in the *z* direction followed by vitrification with minimal chain relaxation.

Drying temperature (Figure 2F): films dried at lower temperatures exhibit higher final birefringence than those dried at higher temperatures. This is counterintuitive because higher temperatures are expected to accelerate solvent evaporation, promoting more in-plane alignment of polymer chains. Indeed, a closer look at the initial increase in birefringence shows that drying at high temperatures initially causes a faster rise in birefringence. However, this rapid initial increase is followed by a significant slowdown in the rate of growth for high-temperature drying, enabling films dried at lower temperatures to catch up and even surpass the birefringence of high-temperature films. This likely occurs because very high drying temperatures lead to rapid solvent loss and the formation of a skin on top of the film, as described in previous work.[45] This skin then impedes further solvent evaporation, causing the rest of the film to dry slowly and allowing more chain relaxation, which results in lower final birefringence.

MW (Figure 2G): with high-MW solutions, OOP birefringence increases more rapidly at first and reaches a higher final value compared to low-MW solutions. This is likely because high-MW polymers have more entanglements, which slow relaxation and result in more oriented chains, than low-MW polymers, which relax faster and have less overall orientation.

These observations collectively highlight that both intrinsic factors (MW) and processing conditions (such as concentration, thickness, and temperature) are crucial in determining the degree of chain orientation in solution-cast pCBDC. Fine-tuning these parameters allows for adjustable control of chain alignment, guiding process strategies for the large-scale production of high-performance films.

## Mechano-optical behavior during uniaxial stretching

### *Stress-strain behavior*

The stress-strain behavior of pCBDC films during uniaxial stretching at different temperatures is shown in Figure 3A. The films show higher yield stress at lower temperatures and an earlier, more pronounced onset of strain hardening. Stretching near the $T_g$ causes significant yielding. Conversely, at very high temperatures, the films exhibit minimal elastic behavior and lack strain hardening. Notably, applying a higher strain rate at a given temperature yields similar results to those obtained with a lower strain rate at lower temperatures, such as more yielding, higher yield stress, and an earlier, more intense onset of strain hardening (see Figure S8 for plots with a lower strain rate). The strain at which strain hardening begins as a function of temperature and strain rate is shown in Figure 4C.

### *Stress-optical behavior*

The stress-optical behavior of pCBDC films during uniaxial stretching is depicted in Figure 3B. Three regions are observed in the stress-birefringence curves (most clearly in the 95°C curve). Region I exhibits photoelastic behavior, where a large amount of stress is needed for a small increase in birefringence. Region II shows a rapid rise in birefringence, with a smaller increase in stress. Region III involves both stress and birefringence increasing together, with the slope gradually decreasing. These regions correspond to the elastic, yielding (or strain-softening), and strain-hardening phases seen in the stress-strain curves. As the temperature increases, the length of region I shortens, and its initial slope becomes steeper. Beyond a certain temperature, regions I and II merge into a single region with a constant slope. Increasing temperature further above this point has little effect on the slope of the combined region, indicating the material has entered the stress-optical-law regime, where a true "unstructured" fluid forms. Figure 4A displays the slopes of regions I (the photoelastic constant) and II at various stretching temperatures and strain rates. The temperature at which these slopes become equal marks the polymer's $T_{II}$, with the slope representing the stress-optical constant: $C = 8.7\ \mathrm{GPa}^{-1}$. $T_{II}$ also depends on strain rate and is approximately ~115°C at 20 mm/min and ~125°C at 200 mm/min.

### *Strain-optical behavior*

Figure 3C illustrates the strain-optical behavior of pCBDC films during uniaxial stretching at different temperatures and strain rates. As the films are stretched, the polymer chains align, exhibiting a linear relationship between strain and birefringence. The slope of this line indicates the strain-optical constant, which represents the connection between macroscopic strain (based on true strain) and the molecular-level strain (the amount of molecular stretching needed for polymer chain alignment as reflected in birefringence). At higher strains, a negative deviation from the linear slope appears as birefringence begins to saturate; further strain no longer significantly increases birefringence, indicating that additional macroscopic strain does not produce more chain alignment because the polymer chains have reached their finite extensibility. As the temperature rises, birefringence increases more gradually with strain. This trend is shown in Figure 4B,

Please cite this article in press as: Davis et al., High-molecular-weight hemp-derived polycannabidiol carbonate thermoplastic with PET-like heat resistance, strength, and processability, Chem Circularity (2026), https://doi.org/10.1016/j.checir.2026.100018



CellPress
OPEN ACCESS

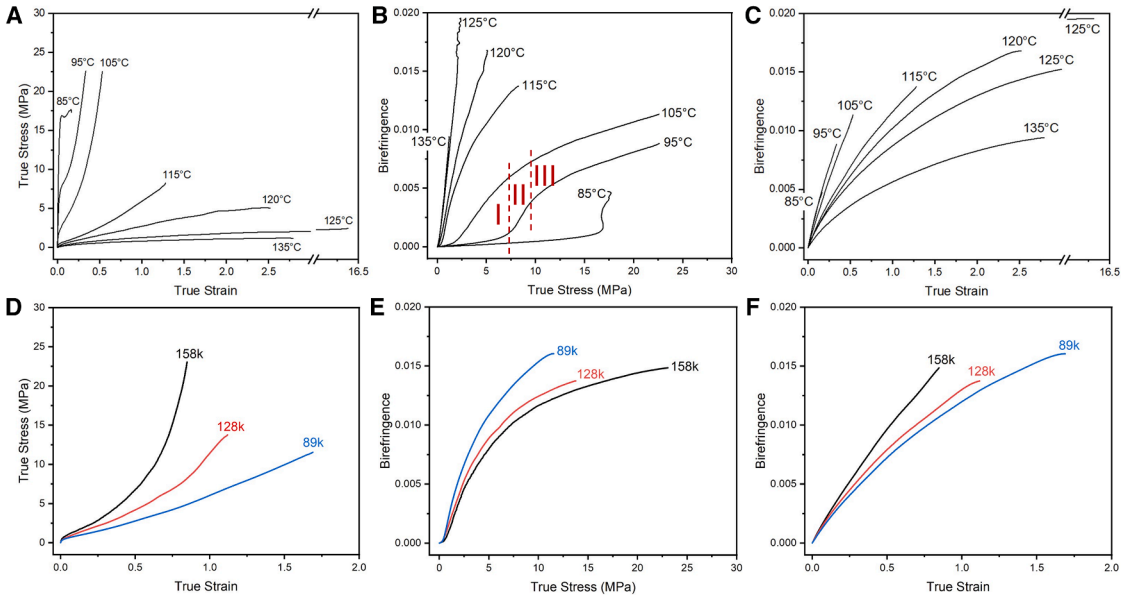


**Figure 3. Mechano-optical behavior of pCBDC films**

(A and D) Stress-strain, (B and E) stress-optical, and (C and F) strain-optical behavior during uniaxial stretching of pCBDC films at 200 mm/min. Plots in (A)–(C) show Mw 158 kDa stretched at various temperatures. In plot (B), regions 1, 2, and 3 are indicated in red on the 95°C curve. Plots in (D)–(F) show various MWs stretched at 110°C. Plots similar to (A)–(C) showing various temperatures but at a strain rate of 20 mm/min are shown in Figure S8.

where the strain-optical constant decreases with increasing temperature. This occurs because higher temperatures lead to more chain relaxation, reducing the degree of chain alignment at a given macroscopic strain. Additionally, lower strain rates generally result in lower strain-optical constants because reducing the strain rate allows more time for chain relaxation, which diminishes chain alignment.

### *Molecular weight effects*

Figures 3D–3F show how MW influences mechano-optical behavior. Although the initial elastic response is similar across

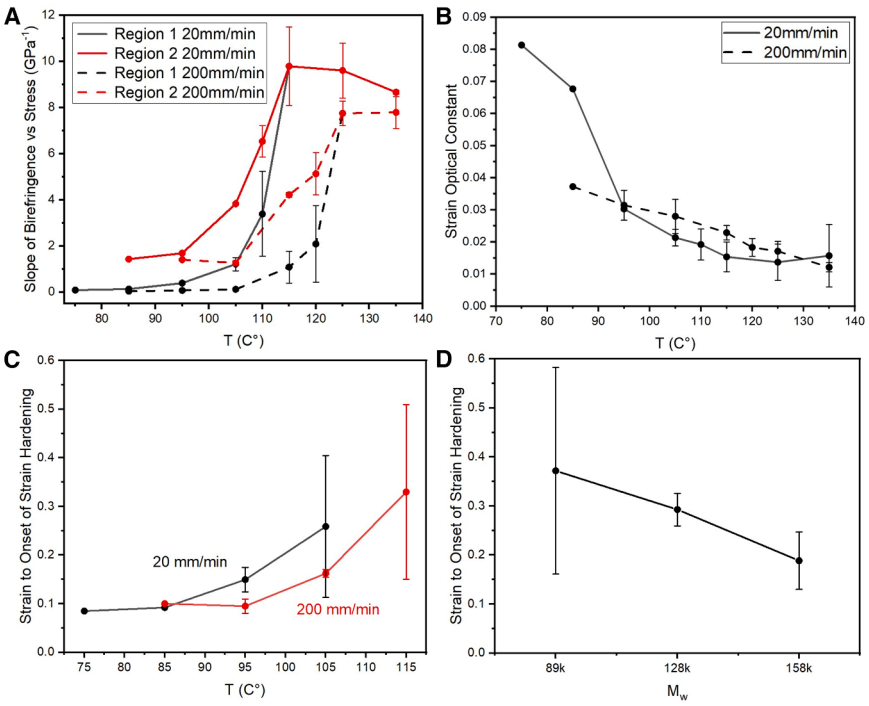


**Figure 4. Stress-optic, strain-optic, and strain-hardening behavior of pCBDC films**

(A) Region 1 and region 2 slope vs. temperature and strain rate.

(B) Strain-optical constant vs. temperature and strain rate.

(C and D) Strain at onset of strain hardening vs. (C) temperature and strain rate and (D) MW.

Please cite this article in press as: Davis et al., High-molecular-weight hemp-derived polycannabidiol carbonate thermoplastic with PET-like heat resistance, strength, and processability, Chem Circularity (2026), https://doi.org/10.1016/j.checir.2026.100018



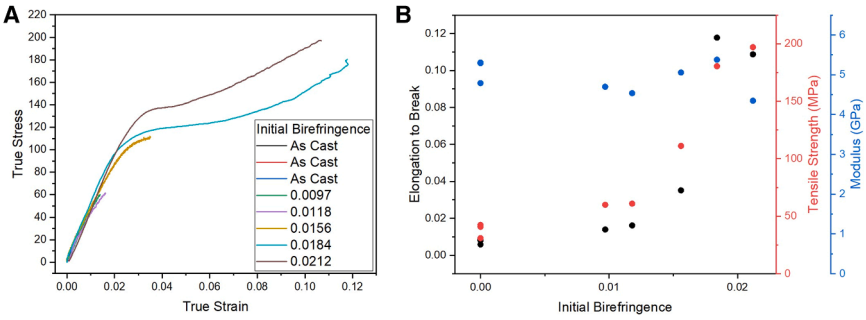


**Figure 5. Effect of orientation on pCBDC film properties**

(A) Stress-strain curves of films with varying initial birefringence during room temperature tensile tests.

(B) Effect of film initial birefringence on mechanical properties.

different MW values, high-MW films display an earlier onset and more pronounced strain hardening. This is because high-MW films have more entanglements that enhance strain hardening. The strain at the onset of strain hardening for each MW is shown in Figure 4D. Additionally, as can be seen in the strain-optical behavior in Figure 3F, high-MW films demonstrate higher birefringence at a given strain compared to low-MW films. This supports the idea that entanglements inhibit relaxation and improve the transfer of strain from the macroscopic to the molecular level. All these factors highlight the importance of high MW for processing and properties of high-performance polymers, and the impressive strain hardening seen with the 158 kDa Mw polymer emphasizes the potential of pCBDC for large-scale processing and use as a sustainable engineering polymer.

## Effect of chain orientation on mechanical properties

To examine the room temperature mechanical properties of pCBDC films and the influence of molecular orientation, films were stretched to various draw ratios (from 2 to 5.5) at 115°C at a rate of 20 mm/min. They were then rapidly cooled to lock in the orientation and subsequently stretched at room temperature to evaluate mechanical properties. Additionally, as-cast films were stretched at room temperature, and the results are compared with the oriented samples in Figure 5. Interestingly, although as-cast samples exhibit brittle behavior at room temperature, films that have been pre-oriented at 115°C are significantly more ductile, with elongation to break increasing with the level of orientation from 0.7% to 11%. This behavior, called a brittle to ductile transition, has been observed in other polymers, including PS and PMMA.[73]

The mechanical properties of both as-cast and oriented pCBDC films under room temperature tensile stretching are compared with PET, PS, PMMA, and PEF in Table 1 and Figure 1F. The pCBDC films exhibit a high modulus even in the unoriented state and comparable tensile strength in the oriented state to those of other materials listed in Table 1.

## Conclusions

This work presents pCBDC as a bio-based thermoplastic derived from hemp-based CBD, emphasizing its potential as a sustainable alternative to petroleum-based engineering polymers. pCBDC is produced via ambient-temperature solution polymerization using crystalline triphosgene, which is completely consumed during the process, yielding an Mw of 158 kDa. The CBD-derived aromatic backbone of pCBDC provides a rare combination of a high $T_g$ (95°C), excellent stretch processability (up to 1,600% strain), and significant hydrophobicity (water contact angle of 102°). Meanwhile, the carbonate linkages are expected to facilitate chemical recycling compatible with current methods for condensation polymers. Beyond synthesis, this study establishes a clear process-structure-property framework that connects processing conditions to polymer chain alignment, offering a rational pathway to tune mechanical, dielectric, and gas-barrier properties without additional chemical modifications. This capacity to improve performance through processing rather than formulation aligns with green chemistry principles by reducing material complexity and additive content. Overall, the inherent properties of pCBDC, combined with its renewable feedstock, position it as a promising bio-based substitute for conventional engineering plastics such as PET, PS, and PMMA in applications including flexible electronics substrates, high-temperature dielectric films, packaging, and fibers. Future work will view the current synthesis and casting methods as a developmental milestone rather than a fixed manufacturing process. Ongoing efforts focus on greener approaches, including $CO_2$-derived intermediates and melt-phase polymerization/processing, to further minimize solvent use and reduce environmental impact. By combining renewable sources with comparable performance and process-driven property control, pCBDC offers a practical route to

**Table 1. Mechanical properties of unoriented and oriented polymer films for different polymers**

| | pCBDC | PET[74] | PS[73] | PMMA[73] | PEF[17] |
|---|---|---|---|---|---|
| Unoriented modulus | ~5 GPa | 1.1 GPa | 1.5 GPa | 1.5 GPa | 2.4 GPa |
| Oriented modulus | ~5 GPa | 5 GPa | 2.7 GPa | 5.8 GPa | – |
| Unoriented tensile strength | 38 MPa | 59 MPa[75] | 46 MPa | 65 MPa | 90 MPa |
| Oriented tensile strength | 197 MPa | 200 MPa | 133 MPa | 227 MPa | – |
| Unoriented elongation to break | 0.7% | 500% | 3.8% | 9.5% | 5.2% |
| Oriented elongation to break | 11% | 60% | 46% | 22% | – |

Oriented properties are measured parallel to the orientation direction. Mechanical properties of uniaxially oriented PEF were not found in the literature.

lessen the environmental footprint of thermoplastics and support the shift toward more sustainable polymer technologies.

## METHODS

### Materials and equipment

CBD was delivered by TN Compounds LLC, and anhydrous DCM, methanol, and pyridine were ordered from Fisher Chemicals. Triphosgene was ordered from Oakwood Chemicals. Toluene for solution casting was purchased from J.T. Baker.

$^1$H-NMR spectra were collected on a Bruker AVANCE 500 MHz spectrometer using deuterated chloroform ($CDCl_3$) as the solvent. Samples were collected with 32–64 scans, depending on concentration, to ensure adequate signal-to-noise ratios.

MW characterization was performed using a Waters GPC system equipped with a 1515 high-performance liquid chromatography (HPLC) pump, 717 Plus autosampler, and refractive index (RI) detector. Polymer samples were dissolved in anhydrous dimethylacetamide (DMAc) at concentrations of 2–4 mg/mL, filtered through 0.45 μm PTFE syringe filters, and injected for analysis. MWs were determined using PS calibration standards with universal calibration.

Differential scanning calorimetry (DSC) measurements were conducted on a TA Instruments DSC Q20 under a nitrogen atmosphere. Samples (4–6 mg) were sealed in aluminum pans and equilibrated at −80°C before being heated to 300°C at a rate of 10°C/min, followed by cooling at the same rate. An initial heating-cooling cycle was used to erase thermal history, and thermal transitions, including the $T_g$, were determined from the second heating cycle. Representative heating and cooling cycles are provided in Figure S4A.

### Solution polymerization and workup

For synthesis of the 158 kDa Mw polymer, a clean and dry 500 mL three-neck round-bottom flask (RBF) was flushed with argon to create an inert atmosphere, and the flask was later sealed with rubber septa on all necks before starting the reaction. A total of 20 g (0.0636 mol) of CBD was put into the flask, followed by the addition of 90 mL of anhydrous pyridine. The solution was stirred for 15 min and placed in a chilled ice bath. Separately, 8.5 g (0.0286 mol) of triphosgene was dissolved in 150 mL of anhydrous DCM in another RBF, forming a clear solution, which was then added dropwise via an addition funnel to the RBF containing the chilled CBD and pyridine solution. The contents were stirred using a magnetic stirrer set at 300 rpm for approximately 20 min in the ice bath and for an additional 4 days with the ice bath removed.

For precipitation, the polymer solution was transferred to a separating funnel and added dropwise to a beaker containing 1 L of methanol, which was continuously stirred with a stirring bar. The precipitated polymer was filtered using a vacuum filter setup, and polymer strands were collected. The filtered polymer was air-dried in a tray overnight and placed in a vacuum oven at room temperature for 1 day to dry completely, yielding 20 g of polymer with a 92% yield. The same synthesis process was followed to obtain the other two MWs. To do this, 8.5 g of triphosgene was replaced with either 6.3 (0.0212 mol, for Mw = 89,000 Da) or 7.42 (0.025 mol, for Mw = 128,000 Da) g.

For future scale-up, greener carbonylating agents such as dimethyl carbonate, diphenyl carbonate, or $CO_2$-derived intermediates are being investigated as alternative routes. Similarly, replacing conventional solvents with more sustainable solvents while ensuring reproducibility and high purity is also currently under evaluation.

### Solution casting and real-time drying analysis

pCBDC was dissolved in toluene at the appropriate concentration (20%–30%), and the solution was cast onto a glass substrate at room temperature using a doctor blade set to the desired thickness (305–610 μm). After casting, the solution was dried at the desired temperature (25°C–65°C) in an instrumented drying system using a heated blower with an airspeed of 1 m/s. During drying, this instrumented system measures real-time film weight, thickness, surface temperature, light transmission, and in-plane and OOP birefringence. The system was custom developed in our laboratories and is shown in Figure S6. It is described in greater detail in previous literature.[76]

### Uniaxial stretching and real-time mechano-optical analysis

Samples for uniaxial stretching were fabricated using a roll-to-roll solution-casting system with a heat-treated PET substrate, a doctor blade, and heaters beneath the substrate. pCBDC material was dissolved in toluene at 25% polymer by weight. For solution casting, the doctor blade gap was 305 μm, the line speed was 100 mm/min, and the heater temperature was 70°C. After casting, the pCBDC film was removed from the substrate and punched into a dumbbell shape for uniaxial stretching. Stretching was performed using a custom-built system shown in Figure S7 and described fully in our previous work.[77] This system is capable of uniaxial stretching at temperatures up to 200°C while simultaneously measuring real-time true stress, true strain, and birefringence. For uniaxial stretching, the system was preheated to the desired stretching temperature, and samples were clamped using metal fixtures, inserted, and preheated for 3 min, after which the clamp fixtures were re-tightened. The samples were then preheated for another 15 min and then stretched at the desired rate (20 or 200 mm/min).

## RESOURCE AVAILABILITY

### Lead contact

Requests for further information and resources should be directed to and will be fulfilled by the lead contact, Mukerrem Cakmak (cakmak@purdue.edu).

### Materials availability

The polymer generated in this study is available from the lead contact with a completed materials transfer agreement.

### Data and code availability

- All data reported in this paper will be shared by the lead contact upon request.
- This paper does not report original code.

## ACKNOWLEDGMENTS

This research was funded by the NSF FMRG Program, grant number 2328262.

## AUTHOR CONTRIBUTIONS

Investigation, H.D.D., P.A., J.M., P.R., A.R.K., V.S., and A.P.; visualization, H.D.D. and P.A.; writing—original draft, H.D.D. and P.A.; writing—review & editing, H.D.D., P.A., G.A.S., and M.C.; conceptualization, G.A.S. and M.C.; funding acquisition, G.A.S. and M.C.; project administration, G.A.S. and M.C.; supervision, G.A.S. and M.C.

## DECLARATION OF INTERESTS

G.A.S. has filed a patent for polycannabidiol polymers under patent number US20210322365A1.

## SUPPLEMENTAL INFORMATION

Supplemental information can be found online at https://doi.org/10.1016/j.checir.2026.100018.

Received: September 29, 2025
Revised: February 11, 2026
Accepted: March 30, 2026

## REFERENCES

1. Rosenboom, J.-G., Langer, R., and Traverso, G. (2022). Bioplastics for a circular economy. Nat. Rev. Mater. *7*, 117–137.
2. Vom Saal, F.S., Antoniou, M., Belcher, S.M., Bergman, A., Bhandari, R.K., Birnbaum, L.S., Cohen, A., Collins, T.J., Demeneix, B., Fine, A.M., et al. (2024). The Conflict between Regulatory Agencies over the 20,000-Fold Lowering of the Tolerable Daily Intake (TDI) for Bisphenol A (BPA) by the European Food Safety Authority (EFSA). Environ. Health Perspect. *132*, 045001.
3. Zimmermann, L., Scheringer, M., Geueke, B., Boucher, J.M., Parkinson, L.V., Groh, K.J., and Muncke, J. (2022). Implementing the EU Chemicals Strategy for Sustainability: The case of food contact chemicals of concern. J. Hazard. Mater. *437*, 129167.
4. Spierling, S., Knüpffer, E., Behnsen, H., Mudersbach, M., Krieg, H., Springer, S., Albrecht, S., Herrmann, C., and Endres, H.J. (2018). Bio-based plastics - A review of environmental, social and economic impact assessments. J. Clean. Prod. *185*, 476–491.
5. Jiang, Y., Maniar, D., Woortman, A.J.J., Alberda Van Ekenstein, G.O.R., and Loos, K. (2015). Enzymatic Polymerization of Furan-2,5-Dicarboxylic Acid-Based Furanic-Aliphatic Polyamides as Sustainable Alternatives to Polyphthalamides. Biomacromolecules *16*, 3674–3685.
6. Rosenboom, J.-G., Hohl, D.K., Fleckenstein, P., Storti, G., and Morbidelli, M. (2018). Bottle-grade polyethylene furanoate from ring-opening polymerisation of cyclic oligomers. Nat. Commun. *9*, 2701.
7. Vouyiouka, S.N., Karakatsani, E.K., and Papaspyrides, C.D. (2005). Solid state polymerization. Prog. Polym. Sci. *30*, 10–37.
8. Luo, K., Wang, Y., Yu, J., Zhu, J., and Hu, Z. (2016). Semi-bio-based aromatic polyamides from 2,5-furandicarboxylic acid: toward high-performance polymers from renewable resources. RSC Adv. *6*, 87013–87020.
9. Weinland, D.H., van der Maas, K., Wang, Y., Bottega Pergher, B., van Putten, R.J., Wang, B., and Gruter, G.J.M. (2022). Overcoming the low reactivity of biobased, secondary diols in polyester synthesis. Nat. Commun. *13*, 7370.
10. Di Lorenzo, M.L. (2024). Crystallization of Poly(ethylene terephthalate): A Review. Polymers *16*, 1975.
11. Menary, G.H., Tan, C.W., Harkin-Jones, E.M.A., Armstrong, C.G., and Martin, P.J. (2012). Biaxial deformation and experimental study of PET at conditions applicable to stretch blow molding. Polym. Eng. Sci. *52*, 671–688.
12. Velasquez, S.T.R., Hu, Q., Kramm, J., Santin, V.C., Völker, C., and Wurm, F.R. (2025). Plastics of the Future? An Interdisciplinary Review on Bio-based and Biodegradable Polymers: Progress in Chemistry, Societal Views, and Environmental Implications. Angew. Chem. Int. Ed. *64*, e202423406.
13. Mekonnen, T., Mussone, P., Khalil, H., and Bressler, D. (2013). Progress in bio-based plastics and plasticizing modifications. J. Mater. Chem. A *1*, 13379.
14. Volanti, M., Cespi, D., Passarini, F., Neri, E., Cavani, F., Mizsey, P., and Fozer, D. (2019). Terephthalic acid from renewable sources: early-stage sustainability analysis of a bio-PET precursor. Green Chem. *21*, 885–896.
15. Sousa, A.F., Patrício, R., Terzopoulou, Z., Bikiaris, D.N., Stern, T., Wenger, J., Loos, K., Lotti, N., Siracusa, V., Szymczyk, A., et al. (2021). Recommendations for replacing PET on packaging, fiber, and film materials with bio-based counterparts. Green Chem. *23*, 8795–8820.
16. De Jong, E., Visser, H.R.A., Dias, A.S., Harvey, C., and Gruter, G.-J.M. (2022). The Road to Bring FDCA and PEF to the Market. Polymers *14*, 943.
17. Stoclet, G., Lefebvre, J.M., Yeniad, B., Gobius Du Sart, G., and De Vos, S. (2018). On the strain-induced structural evolution of Poly(ethylene-2,5-furanoate) upon uniaxial stretching: An in-situ SAXS-WAXS study. Polymer *134*, 227–241.
18. Visković, J., Zheljazkov, V.D., Sikora, V., Noller, J., Latković, D., Ocamb, C.M., and Koren, A. (2023). Industrial Hemp (Cannabis sativa L.) Agronomy and Utilization: A Review. Agronomy *13*, 931.
19. Adesina, I., Bhowmik, A., Sharma, H., and Shahbazi, A. (2020). A Review on the Current State of Knowledge of Growing Conditions, Agronomic Soil Health Practices and Utilities of Hemp in the United States. Agriculture *10*, 129.
20. Nath, M.K. (2022). Benefits of Cultivating Industrial Hemp (Cannabis sativa ssp. sativa)—A Versatile Plant for a Sustainable Future. Chem. Proc. *10*, 14. https://doi.org/10.3390/IOCAG2022-12359.
21. Gill, A.R., Loveys, B.R., Cavagnaro, T.R., and Burton, R.A. (2023). The potential of industrial hemp (Cannabis sativa L.) as an emerging drought resistant fibre crop. Plant Soil *493*, 7–16.
22. Scalabrin, E., Radaelli, M., Capodaglio, G., Pierobon, M., Del Vecchio, S., and Buffa, G. (2024). Hemp cultivation opportunities for marginal lands development. PLoS One *19*, e0299981.
23. Gorchs, G., Lloveras, J., Serrano, L., and Cela, S. (2017). Hemp Yields and Its Rotation Effects on Wheat under Rainfed Mediterranean Conditions. Agron. J. *109*, 1551–1560.
24. Enarevba, D.R., and Haapala, K.R. (2024). The Emerging Hemp Industry: A Review of Industrial Hemp Materials and Product Manufacturing. AgriEngineering *6*, 2891–2925.
25. Davidson, M.G., Elgie, S., Parsons, S., and Young, T.J. (2021). Production of HMF, FDCA and their derived products: a review of life cycle assessment (LCA) and techno-economic analysis (TEA) studies. Green Chem. *23*, 3154–3171.
26. Fonseca, A., Ramalho, E., Gouveia, A., Figueiredo, F., and Nunes, J. (2023). Life Cycle Assessment of PLA Products: A Systematic Literature Review. Sustainability *15*, 12470.
27. Kaur, G., and Kander, R. (2023). The Sustainability of Industrial Hemp: A Literature Review of Its Economic, Environmental, and Social Sustainability. Sustainability *15*, 6457.
28. Law Library of Congress (2022). Regulation of Hemp (Global Legal Research Directorate). https://tile.loc.gov/storage-services/service/ll/llglrd/2022666115/2022666115.pdf.
29. DeCarlo, S. & Weaver, M. Keeping the High Out of Hemp: Global THC Standards. (2023).
30. Kościuszko, A., Rojewski, M., Nowinka, B., and Patalas, F. (2022). Post-Molding Shrinkage, Structure and Properties of Cellular Injection-Molded Polypropylene. Materials *15*, 7079.

31. Carrupt, M.C., and Piedade, A.P. (2021). Modification of the Cavity of Plastic Injection Molds: A Brief Review of Materials and Influence on the Cooling Rates. Materials *14*, 7249.

32. Daniels, R., Morato, E.O., Yassin, O.A., Mao, J., Mutlu, Z., Jain, M., Valenti, J., Cakmak, M., Nair, L.S., and Sotzing, G.A. (2022). Poly(cannabinoid)s: Hemp-Derived Biocompatible Thermoplastic Polyesters with Inherent Antioxidant Properties. ACS Appl. Mater. Interfaces *14*, 42804–42811.

33. Selvaraj, S., Nawfer, N., Dharmawansa, K.V.S., Ali Redha, A., and Rupasinghe, H.P.V. (2025). Recent advances in cannabidiol (CBD) extraction: a review of potential eco-friendly solvents and advanced technologies. Green Anal. Chem. *13*, 100270.

34. HempBenchmarksSpotPriceIndexReport-July2023. 2023

35. IMARC Group (2025). Polyethylene Terephthalate (PET) Prices, Trend, Chart, Demand, Market Analysis, News, Historical and Forecast Data Report 2025 Edition (IMARC Group). https://www.imarcgroup.com/polyethylene-terephthalate-pricing-report.

36. Ouyang, W., Ou, J., Zheng, Q., Yang, X., Meng, Y., Du, G., Liu, F., Chen, Y., and Tang, K. (2025). Agronomic evaluation of hemp (Cannabis sativa L.) for cannabidiol production in Yunnan, China. Front. Agron. *7*, 1539426.

37. IMARC Group (2024). Polyethylene Furanoate Pricing Report 2024: Price Trend, Chart, Market Analysis, News, Demand, Historical and Forecast Data (' IMARC Group). https://www.imarcgroup.com/polyethylene-furanoate-pricing-report.

38. Boersma, A., Cangialosi, D., and Picken, S.J. (2003). Mobility and solubility of antioxidants and oxygen in glassy polymers. III. Influence of deformation and orientation on oxygen permeability. Polymer *44*, 2463–2471.

39. De Vries, A.J., Bonnebat, C., and Beautemps, J. (1977). Uni- and biaxial orientation of polymer films and sheets. J. polym. sci. C. Polym. symp. *58*, 109–156.

40. Forshey, M. Orientation of Polymer Films for Improvement of Dielectric Properties for High-Energy Density Capacitor Applications. (2019).

41. Prest, W.M., and Luca, D.J. (1979). The origin of the optical anisotropy of solvent cast polymeric films. J. Appl. Phys. *50*, 6067–6071.

42. Prest, W.M., and Luca, D.J. (1980). The alignment of polymers during the solvent-coating process. J. Appl. Phys. *51*, 5170–5174.

43. Eguchi, Y., Unsal, E., and Cakmak, M. (2013). Critical Phenomenon During Drying of Semiaromatic, Transparent and Soluble Polyimide Cast Films: Real-Time Observation of Birefringence and Other Integrated Parameters. Macromolecules *46*, 7488–7501.

44. Unsal, E., and Cakmak, M. (2013). Real-Time Characterization of Physical Changes in Polyimide Film Formation: From Casting to Imidization. Macromolecules *46*, 8616–8627.

45. Yucel, O., Unsal, E., and Cakmak, M. (2013). Temporal Evolution of Optical Gradients during Drying in Cast Polymer Solutions. Macromolecules *46*, 7112–7117.

46. Jiang, F., and Cakmak, M. (2015). Real time optical and mechano-optical studies during drying and uniaxial stretching of Polyetherimide films from solution. Polymer *68*, 168–175.

47. Van Melick, H.G.H., Govaert, L.E., and Meijer, H.E.H. (2003). On the origin of strain hardening in glassy polymers. Polymer *44*, 2493–2502.

48. Seif, S., and Cakmak, M. (2010). Stress - Optical behavior of Poly(m-xylylenediamine adipamide) (Nylon MXD6): Influence of molecular weight. Polymer *51*, 3762–3773.

49. Govaert, L.E., and Tervoort, T.A. (2004). Strain hardening of polycarbonate in the glassy state: Influence of temperature and molecular weight. J. Polym. Sci. B Polym. Phys. *42*, 2041–2049.

50. Haward, R.N. (1993). Strain hardening of thermoplastics. Macromolecules *26*, 5860–5869.

51. (1968). The use of a mathematical model to describe isothermal stress-strain curves in glassy thermoplastics. Proc. R. Soc. Lond. Ser. Math. Phys. Sci. *302*, 453–472.

52. Coates, P.D., and Ward, I.M. (1980). Neck profiles in drawn linear polyethylene. J. Mater. Sci. *15*, 2897–2914.

53. Zhou, X., and Cakmak, M. (2007). Stress–strain behavior as related to surface topography and thickness uniformity in uni- and biaxially stretched PVDF/PMMA blends. Polym. Eng. Sci. *47*, 2110–2117.

54. Cakmak, M., and Simhambhatla, M. (1995). Dynamics of uni and biaxial deformation and its effects on the thickness uniformity and surface roughness of poly (ether ether ketone) films. Polym. Eng. Sci. *35*, 1562–1568.

55. Iwakura, K., Wang, Y.D., and Cakmak, M. (1992). Effect of Biaxial Stretching on Thickness Uniformity and Surface Roughness of PET and PPS Films. Int. Polym. Process. *7*, 327–333.

56. Mutlu, Z., Jain, M., Yook, S.H., and Cakmak, M. (2021). Mechano-optical behavior in poly (ethylene terephthalate)/poly (ether imide) blends. J. Polym. Sci. *59*, 2045–2056.

57. Chen, K., Dreger, N.Z., Peng, F., Vogt, B.D., Becker, M.L., and Cakmak, M. (2018). Nonlinear Mechano-Optical Behavior and Strain-Induced Structural Changes of l - Valine-Based Poly(ester urea)s. Macromolecules *51*, 8114–8126.

58. (1997). The Physics of Glassy Polymers (Springer Netherlands). https://doi.org/10.1007/978-94-011-5850-3.

59. Steger, T.R., and Nielsen, L.E. (1978). Microvoid formation during deformation of high-impact polystyrene. J. Polym. Sci. Polym. Phys. Ed. *16*, 613–625.

60. Boyer, R.F. (1987). Evidence from T ll and Related Phenomena for Local Structure in the Amorphous State of Polymers. In Order in the Amorphous "State" of Polymers, S.E. Keinath, R.L. Miller, and J.K. Rieke, eds. (Springer US), pp. 135–185. https://doi.org/10.1007/978-1-4613-1867-5_7.

61. Boyer, R.F. (1980). Dynamics and thermodynamics of the liquid state ($T < T_g$) of amorphous polymers. J. Macromol. Sci. Part B *18*, 461–553.

62. Lobanov, A.M., and Frenkel', S. (1980). The nature of the so-called "liquid-liquid" transition in polymer melts. A review. Polym. Sci. USSR *22*, 1150–1163.

63. Barthlott, I., Scharinger, A., Golombek, P., Kuballa, T., and Lachenmeier, D.W. (2021). A Quantitative 1H NMR Method for Screening Cannabinoids in CBD Oils. Toxics *9*, 136.

64. Sawada, R., Liu, H., Yanagimoto, S., Yanagimoto, Y., and Ando, S. (2025). Extremely Low Humidity and Frequency Dependence of Dielectric Properties of Highly Fluorinated Polyimides in the 10–330 GHz Range. ACS Appl. Polym. Mater. *7*, 14371–14381.

65. Kurihara, K., Hokari, R., and Takada, N. (2021). Capillary Effect Enhancement in a Plastic Capillary Tube by Nanostructured Surface. Polymers *13*, 628.

66. Parida, D., Aerts, A., Vargas Perez, L., Marquez, C., Vloemans, S., Vanbroekhoven, K., Feghali, E., and Elst, K. (2024). Boosting methanolysis of polycarbonate (PC) for bisphenol A recovery from end-of-life PC and PC/ABS blend. Chem. Eng. J. *497*, 154390.

67. Lee, E., Moon, I., and Kim, J. (2025). Optimal industrial-scale recycling strategy for polycarbonate via alcoholysis: Evaluation of techno-economics and greenhouse gas emissions. Chem. Eng. J. *519*, 164400.

68. Lee, H.W., Yoo, K., Borchardt, L., and Kim, J.G. (2024). Chemical recycling of polycarbonate and polyester without solvent and catalyst: mechanochemical methanolysis. Green Chem. *26*, 2087–2093.

69. Saito, K., Eisenreich, F., and Tomović, Ž. (2024). Multi-Pathway Chemical Recycling of Bio-Based Polycarbonates Containing Spirocyclic Acetal Structures. Macromolecules acs macromol *57*, 8690. https://doi.org/10.1021/acs.macromol.4c01553.

70. Zhang, M., and Wu, Y. (2025). Advancing chemical recycling for waste plastic conversion. Cell Rep. Phys. Sci. *6*, 102910.

71. Chin, M.T., and Diao, T. (2024). Industrial and Laboratory Technologies for the Chemical Recycling of Plastic Waste. ACS Catal. *14*, 12437–12453.

72. Clark, R.A., and Shaver, M.P. (2024). Depolymerization within a Circular Plastics System. Chem. Rev. *124*, 2617–2650.

73. Zartman, G.D., Cheng, S., Li, X., Lin, F., Becker, M.L., and Wang, S.Q. (2012). How Melt-Stretching Affects Mechanical Behavior of Polymer Glasses. Macromolecules *45*, 6719–6732.

74. Cakmak, M. Dynamics and structure development in biaxially stretched polyethylene terephthalate films and stretch blow molded bottles. PhD thesis (University of Tennessee). 1984. https://trace.tennessee.edu/utk_graddiss/12838

75. Polymerfilms-NanYaPlastics-APET-APBM-Datasheet. https://polymerfilms.com/wp-content/uploads/2023/07/Polymerfilms-NanYaPlastics-APET-APBM-Datasheet.pdf

76. Unsal, E., Drum, J., Yucel, O., Nugay, I.I., Yalcin, B., and Cakmak, M. (2012). Real-time measurement system for tracking birefringence, weight, thickness, and surface temperature during drying of solution cast coatings and films. Rev. Sci. Instrum. *83*, 025114.

77. Koike, Y., and Cakmak, M. (2003). Real time development of structure in partially molten state stretching of PP as detected by spectral birefringence technique. Polymer *44*, 4249–4260.